

Modelling Consequences of Artificial Structures on Salt Marsh Dynamics in the Wadden Sea

R.W.A. Siemes; 2019



**UNIVERSITY
OF TWENTE.**

HKV
LIJN IN WATER

Modelling Consequences of Artificial Structures on Salt Marsh Dynamics in the Wadden Sea

Master Thesis

Water Engineering & Management

Faculty of Engineering Technology

University of Twente

Author

Rutger Siemes

Graduation committee

Prof. Dr. S.J.M.H. Hulscher

University of Twente

Dr. Ir. B.W. Borsje

University of Twente

Ir. R.J. Daggenvoorde

HKV

Delft, December 2019

**UNIVERSITY
OF TWENTE.**



Preface

Hereby I present the results of my master thesis. This work is performed in partial fulfilment of the requirements for the Master of Science degree in Water Engineering and Management at the University of Twente, in collaboration with HKV. It is presented in paper format and which will be submitted later this year.

Writing this preface marks the end of the past 7 months in which I worked on this thesis. In retrospect I am glad to say that I truly enjoyed the process and it was a great experience overall.

Without the help and support of various people, this thesis would not have been the work it is now. Therefore, I would like to thank Suzanne Hulscher for her encouragement and constructive criticism during the final stages. I would like to thank Bas Borsje for his enthusiasm throughout the process and for the dynamic discussions at the critical moments during this research, but also for the opportunity to work on this project. Roy Daggenvoorde, thank you for the involvement with my thesis. By thinking along and asking the right questions you often steered me in the right direction. Finally, I would like to thank my family, friends and colleagues for the encouraging and supportive environment that they provided during the graduation process.

Rutger Siemes,

Enschede, 9 December, 2019

Contents

PREFACE	I
ABSTRACT	1
1. INTRODUCTION	2
2. METHODS	4
2.1. STUDY AREA AND FIELD OBSERVATIONS	4
2.2. DELFT3D FLEXIBLE MESH DESCRIPTION	7
2.3. MODEL SETUP	8
2.3.1. <i>Domain and time frame</i>	8
2.3.2. <i>Hydrodynamics</i>	11
2.3.3. <i>Sediment dynamics</i>	12
2.4. ADDITION OF ARTIFICIAL STRUCTURES	14
3. RESULTS	16
3.1. HYDRODYNAMICS	16
3.2. MORPHODYNAMICS	17
3.2.1. <i>Simulated bed-level change</i>	17
3.2.2. <i>Sensitivity analysis</i>	18
3.3. IMPACT OF ARTIFICIAL STRUCTURES	21
4. DISCUSSION	24
4.1. ASSUMPTIONS AND UNCERTAINTIES.....	24
4.2. DEFAULT SIMULATION.....	25
4.3. ARTIFICIAL STRUCTURES	26
4.4. GENERAL APPLICABILITY	28
5. CONCLUSION	29
APPENDIX	30
A VALIDATION OF HYDRODYNAMICS.....	30
A.1. <i>Flow module</i>	30

<i>A.2. Wave module</i>	30
B. INPUT PARAMETERS STRUCTURE IMPLEMENTATION	31
REFERENCES	32

Abstract

Salt marshes are more and more recognized as resilient and sustainable supplements to traditional engineering structures for protecting coasts against flooding. Nevertheless, many salt marshes face severe erosion. There is a general consensus that creating an area which is sheltered from high energetic conditions can improve the potential for salt marsh growth. However, little proof is provided on the explicit influence of structures to promote salt marsh growth. This paper investigates how engineering solutions can be used to steer the morphological development of salt marshes. A morphological model (Delft3D Flexible Mesh) was applied which enables the analysis of various human interventions. A small salt marsh in the Wadden Sea was modelled. This marsh has seen heavy erosion (retreat rate of $0.9m/year$) since maintenance of its sedimentation field and groyne was halted. In the model, we simulate both daily conditions and storm conditions. The model performed well in simulating the hydrodynamic conditions. Key processes relevant for the morphological development of salt marshes are captured and several simulated morphological patterns are observed and identified in literature. The model simulations showed that, without artificial structures erosion of the salt marsh and tidal flat occurs. Results with structures implemented indicated that there is potential for salt marsh growth in the study area. More broadly, results show that a salt marsh accretes during storm events, demonstrating that salt marsh systems may provide a resilient way to supplement hard structures to improve coastal safety in the face of the increasing storminess. In addition, the paper indicates how morphological development of a salt marsh can be steered by implementing various artificial structures.

1. Introduction

Salt marshes are vegetated foreshores which occur at sheltered muddy coast lines such as estuaries or intertidal zones in temperate latitudes. These vegetated foreshores have the ability to attenuate waves and stabilize the bed (Vuik et al., 2016; Willemsen et al., 2018). Furthermore, research has indicated that they are able, within limits, to keep up with a rising sea level (Best et al., 2018). In addition to providing coastal-safety benefits, they also provide ecological benefits by supporting a more diverse biota. Moreover, by providing organic material and nutrient cycling, they function as carbon sinks (Chmura et al., 2003) which makes salt marshes among the most valuable ecosystems on earth (Costanza et al., 1997). In light of these characteristics, stimulation of salt marsh growth can offer a resilient and sustainable supplement to traditional engineering structures for protecting coasts against flooding (Vuik et al., 2019).

Though the benefits of vegetated foreshores are more and more recognized, many foreshores, including salt marshes, suffer erosion (Chang et al., 2016; Millard et al., 2013). While the erosion rate of a salt marsh cliff exhibits a linear relation with wave power (Leonardi et al., 2016), the start of erosion is linked to having a stable marsh next to a dynamic tidal flat. Consequently, a cliff can develop at the marsh front which is attacked by wave action resulting in erosion (Bouma et al., 2016).

The start of salt marsh expansion is characterized by seedling establishment or clonal shoots. Hereby, vegetation stabilizes the bed and functions as a sediment trap. For seedling establishment to succeed, conditions should be such that uprooting or burying of the seedlings is prevented (Hu et al., 2015). The indicating parameters for these conditions are the bed elevation in relation to water level (influencing inundation frequency and period), and bed-level change. Clonal expansion is affected mainly by inundation period and wave and flow energy at the tidal flat (Silinski et al., 2016). The start of salt marsh growth can thus be stimulated by improving the aforementioned conditions at the tidal flat in front of the marsh, for either clonal shoots or seedling establishment.

Thus, creating an area sheltered from high energy conditions can improve the potential for vegetation establishment and hence for salt marsh growth (Poppema et al., 2019). However, little research is performed on how human interventions can be applied to promote salt marsh growth. Van Loon-Steensma and Slim (2012) investigated the biodiversity that occurs on salt marshes which are restored with the aid of groynes. Dao et al. (2018) investigated the wave-damping effect of brushwood groynes, which are often applied to stimulate salt marsh growth. In addition, the long-term cost effectiveness of ecological engineering methods for vegetated foreshores are assessed (Vuik et al., 2019). Hereby bed-level changes on the foreshore are based on spatially uniform accretion scenarios. However, research on implementing artificial structures to steer morphological development within salt marshes is still lacking.

Research on the morphological development of vegetated foreshores is predominantly performed by field- or modelling studies. While field studies can give detailed insight into the conditions that cause bed-level change (Schuerch et al., 2019; Willemsen et al., 2018), this method can be expensive and does

not lend itself well for to the study of long-term morphological developments. Morphological models can be used to study these long-term developments. Moreover, with the ability to alter input characteristics, the impact of individual processes and varying scenarios can be analysed efficiently (Best et al., 2018; Poppema et al., 2019). Similarly, modelling also offers the possibility to assess a range of configurations of engineering structures as well. Therefore, applying a morphological model fits well when researching engineering solutions. It should be considered, however, that models are simplified representations of reality and contain various sources of uncertainty (Haff, 1996). These uncertainties can be reduced by validating model results with field data.

The aim of this paper is to investigate how engineering solutions can be applied to steer the morphological development of salt marshes. This will be achieved by, 1) analysing the dynamic processes motivating morphological development on and around a salt marsh and 2) studying the impact of human interventions on these processes. A process-based numerical model is developed in Delft3D Flexible Mesh (D3D-FM) in which accurate bed levels and hydrodynamic forcing are applied to simulate a month with both daily conditions and storm conditions. A small salt marsh in the Wadden Sea is selected as case study (*Figure 5*). This marsh has suffered heavy erosion ($0.9m/year$) since maintenance of its sedimentation fields and groyne was halted. Also, based on local flow and sediment characteristics, salt marsh stimulation is expected to require large efforts within the area (Loon-Steensma, Groot, et al., 2012). Furthermore, local authorities desire the growth of this salt marsh for cultural, recreational and environmental purposes, thereby giving this study both scientific and practical relevance.

The outline of this paper is as follows. Section 2 describes the study area and the setup of the morphological model applied within this study. In Section 3, the hydrodynamic results are presented and validated after which the morphological results presented as well. Next, model outputs including human interventions are addressed. In the fourth section, the model setup and results are discussed, starting with the hydrodynamics. Consequently, in Section 4, the assumptions and uncertainties within the model setup are discussed, followed by the morphological results with – and without artificial structures. The applicability of this paper is also addressed. In Section 5 the conclusion is presented.

2. Methods

2.1. Study area and field observations

The study area is located in the Wadden Sea, south of the tidal inlet between Ameland and Schiermonnikoog (Figure 5.b). The study area contains a salt marsh and the tidal flat in front of the marsh, up to 1km seawards (Figure 5.c). Hereby, and throughout this paper, the salt marsh is denoted as the area with a bed-level above 0.7 m N.A.P., the marsh front is the area of the marsh with a bed-level between 0.7-1.2 m N.A.P. and the tidal flat includes the rest of the study area.

Tides in the area are predominantly semi-diurnal with an averaged amplitude of 1.1 m and the amplitude of a spring-neap cycle is 0.35 m. Local flow velocities of up to 1.2 m/s are observed (Zwarts et al., 2004). In this paper, the month of October 2017 is simulated which contains both storm conditions and daily conditions. Observed water levels and wind velocities and directions within this period are displayed in Figure 1. Relatively calm conditions occurred between days 9-22 and two storms occurred between days 5-6 and 28-29. During these storms, water levels reach up to 2.5 m N.A.P. and wind speeds reach 23 m/s. On average, based on local observations of the past 30 years, these water levels are exceeded 1.5 times annually (RWS, 2019). The wind speeds are exceeded ones per year (KNMI, 2019).

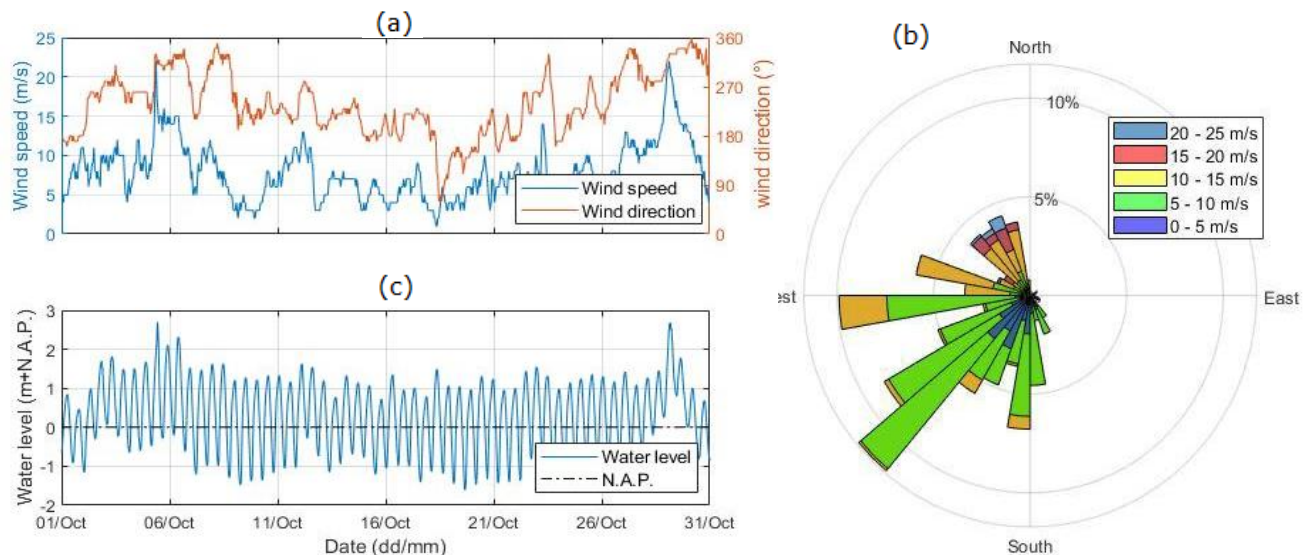


Figure 1. Observed hydrodynamic conditions during the simulated period nearby the study area. Displaying (a) wind velocities and directions at measurement station 'Wierummerwad' over time, (b) a wind rose of wind data at measurement station 'Wierummerwad', and (c) observed water level at measurement station 'Lauwersoog' over time.

Measurements of local bed material show median grain sizes (D_{50}) ranging from 100-180 μm (Deltares, 2015a) and 5-18% of the sediment consists of mud (p_m) (Zwarts et al., 2004). The salt marsh was growing during most of the 19th century after a groyne and sedimentation field were constructed (Figure

3). These sedimentation fields are a human intervention used to stimulate salt marsh growth. They consist of brushwood groynes which enclose areas of a marsh and tidal flat with the exception of small openings. This limits flow and wave energy within the area and, consequently, local sedimentation increases leading to marsh growth. However, after maintenance of these structures was halted, and the structures started to deteriorate, the salt marsh started to erode. Observed bed-level changes between 2008 and 2014 are visualized in Figure 2. The data exhibits an erosion rate of the salt marsh, the area with a bed-level above 0.7 m *N.A.P.*, of $1.1 \text{ m}^3/\text{m}/\text{year}$ averaged along the marsh length. This erosion is mostly in the form of cliff erosion at the marsh front. The data additionally shows a retreat rate of the marsh edge due to the cliff erosion of $0.9 \text{ m}/\text{year}$ averaged along the marsh length.

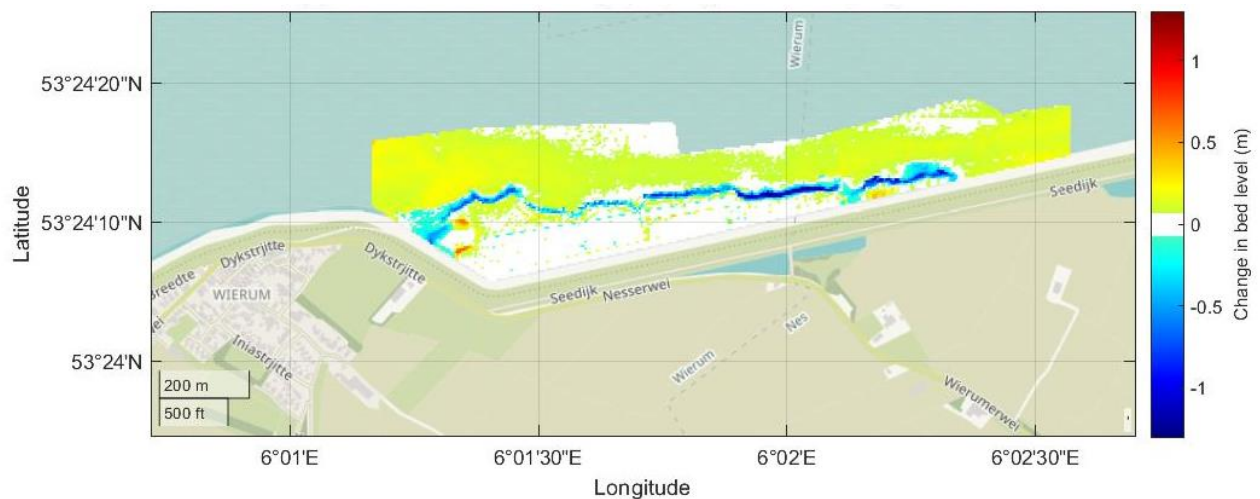


Figure 2. Observed bed-level change between the spring of 2008 and the spring of 2014.



Figure 3. Satellite image of the eroding salt marsh of the study area, near Wierum. Remains of the old sedimentation fields and groyne can still be observed on the tidal flat.

2.2. Delft3D Flexible Mesh description

A model is developed for the study area and its surroundings (*Figure 5.b*). The purpose of the model is twofold. First, the model is used 1) to study the processes that influence bed-level change on an eroding marsh and, consequently, 2) to determine how configurations of engineering structures can be applied to improve hydrodynamic conditions to stimulate salt marsh growth.

A process-based numerical model was developed with D3D-FM in which both a flow and wave module were applied. Within the flow module, the hydrodynamics are solved by using the 2D depth-averaged unsteady shallow-water equations. For the impact of wind on the flow module, the Charnock formulation was applied (Charnock, 1955). Within the wave module, waves are described based on the third-generation SWAN model, which considers wave propagation, wave-breaking, diffraction, refraction, wind growth and frequency shifting (Booij et al., 1999).

Sediment transport and bed-level change is determined based on the formulation of Van Rijn (1993). This formulation was selected since it displayed the best results with initial model testing. The formulation distinguishes transport below and above a reference level, which are bed-load and suspended-load transport, respectively. Sediment advances through the flow based on the computed reference concentration at this reference level. The method initially determines the magnitude of total bed-load transport, which is assumed to be comprised of two parts—current- and flow-related—which are subsequently computed based on total bed-load transport. Their directions are equal to the directions of the near-bed current and wave propagation, respectively (Van Rijn, 1993). For suspended sediment transport, the wave-related component is computed (Van Rijn, 2000). In D3D-FM, the current-related component is not incorporated. Based on the sediment transport, bed-level change is determined. This is performed with source and sink terms where erosion is due to the upward diffusivity of sediment and deposition is due to sediment settling.

In *Figure 4*, a schematization is shown which visualizes how the processes introduced within this section interact with each other. For the simulation we chose input parameters which are typical for a Wadden-Sea location. An overview of these input parameters is shown in *Table 1*.

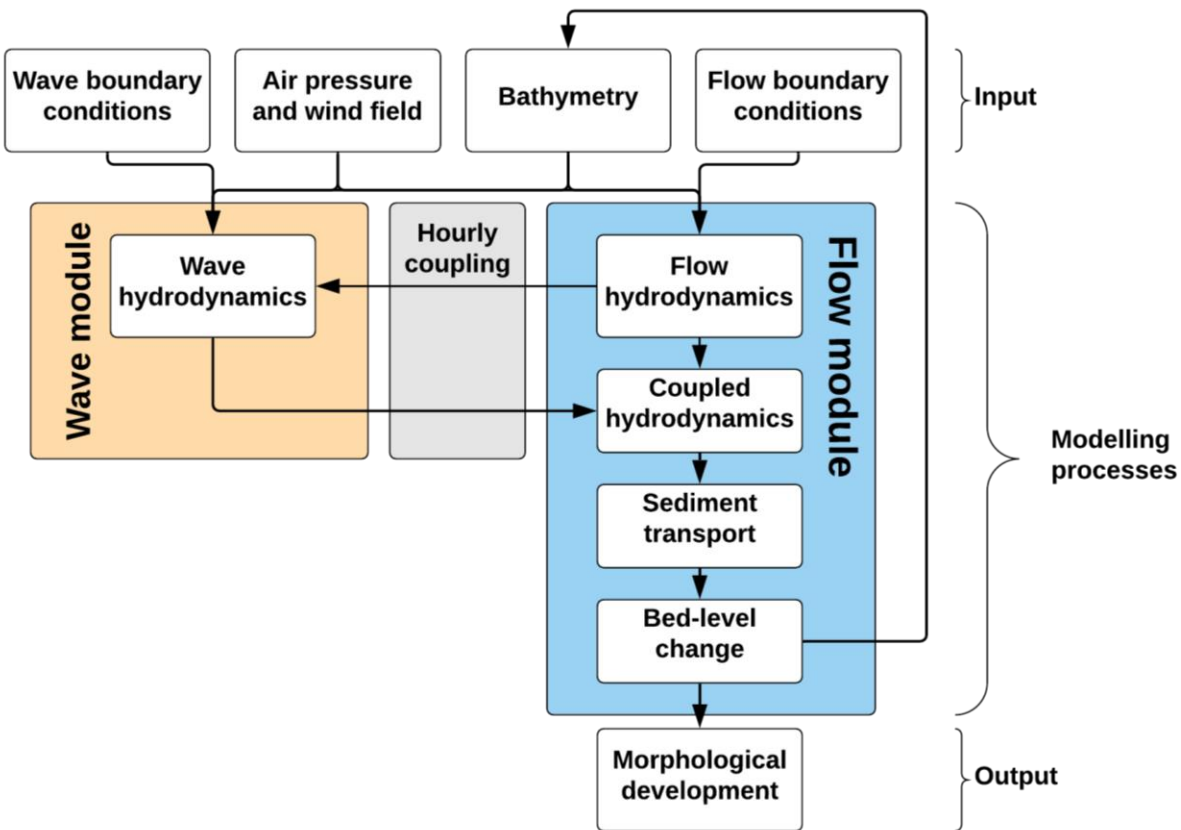


Figure 4. Schematization of processes introduced in Sections 2.2 and 2.3 and how these processes interact with each other in Delft3D Flexible Mesh. Arrows indicate the flow of data. The computational time step within the wave module is hourly. For the flow module, this is equal to the numerical time step. Arrows through the 'hourly coupling' section indicate the communication of data between the modules, which is performed hourly.

2.3. Model setup

2.3.1. Domain and time frame

The model consists of separate domains for the wave and flow modules. The flow domain includes an area of 80 by 50km in which the study area is centred. At the outer edge of the domain, the resolution is 800 by 800m and the grid is refined in four steps towards the study area. The first and fourth refinement steps are with a factor 4 and the second and third with a factor 2, for a total refinement of factor 64. This results in a grid size of 12.5 by 12.5m within the area of interest, which is 5 by 2km. The grid is made up of mostly squares, with triangles along the refinement locations. Within the wave module, a curvilinear grid is applied. The grid has a resolution of 2 by 3km at the northern edges which reduces towards the study area where grid sizes are 150 by 150m. The domain areas and their main characteristics are visualized in Figure 5.b. In both domains diked areas, including the dikes themselves, are flow and wave restricted.

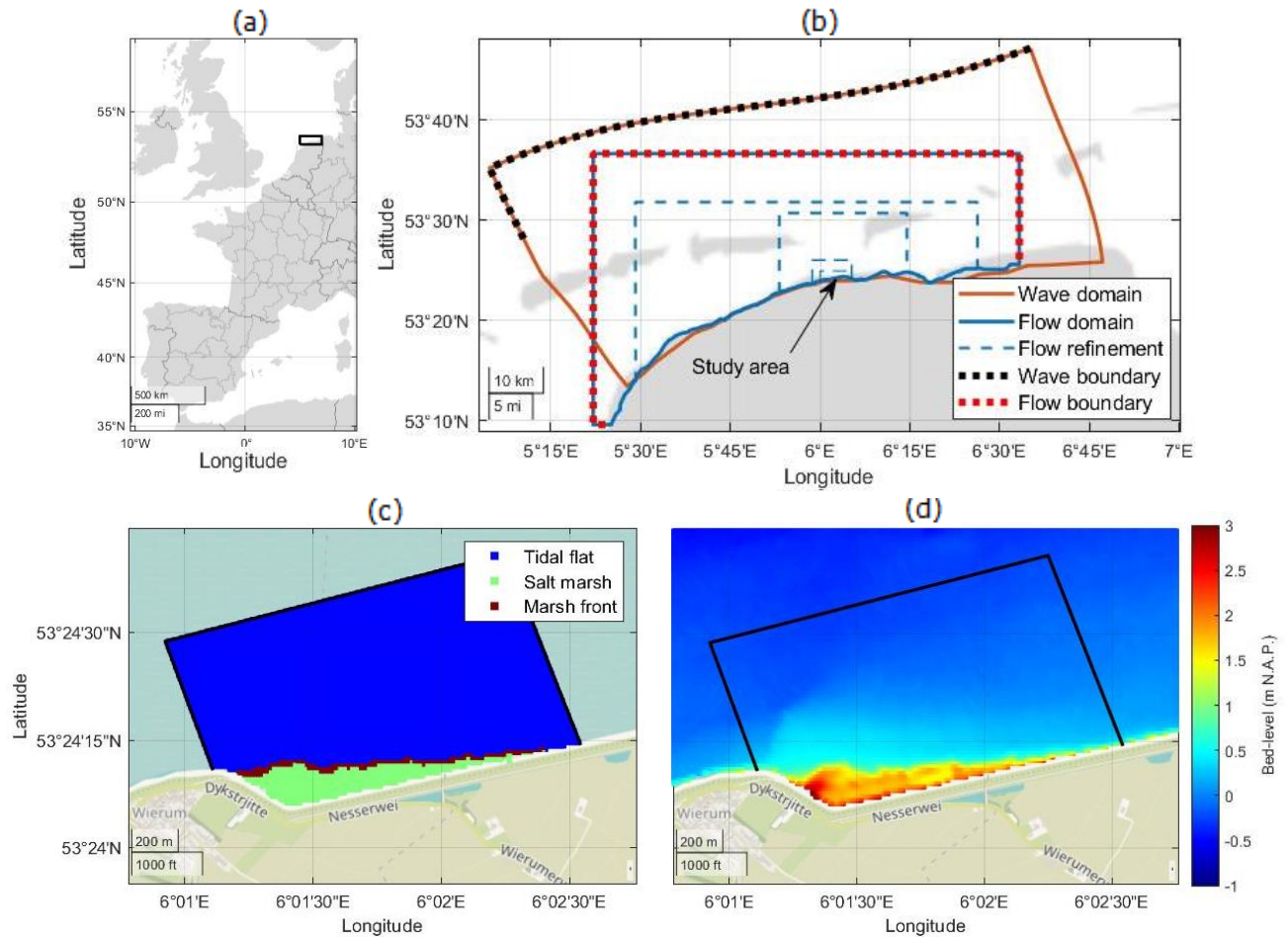


Figure 5. (a) The study area's location within Europe. (b) The area of the model domains and their main characteristics. (c) The location of the tidal flat, salt marsh and marsh front within the study area. The marsh front is also part of the salt marsh itself. (d) The location of the study area (boxed) and its bathymetry within the model. The study area is along the length of the marsh and up to 1km away from the coast.

The area encompassed by the outer refinement step of the flow domain has bathymetry data obtained from the publicly available Open Earth data set (Deltares, 2015b). Bathymetric data for the remaining domain area originates from the Netherlands Hydrographic Office (NLHO, 2013). The bathymetry of the study area is displayed in Figure 5.d. Within the flow domain, a spatially varying Manning coefficient is used for the bed-roughness. Most of the domain has a Manning coefficient of $0.021 s m^{-1/3}$, as derived by Zijl et al. (2013). However, on the salt marsh vegetation is present in the form of a grassy top which increases the bed-roughness. In the model, this vegetation is represented with a manning coefficient of $0.04 s m^{-1/3}$ (Wamsley et al., 2010). The bed-roughness applied within the wave module is determined through calibration, which is discussed in Section 2.3.2.

Furthermore, an eddy viscosity and diffusivity are implemented for the flow module's turbulence model. Since the horizontal eddy viscosity should vary depending on grid size, this value should vary spatially

within the model domain (Deltares, 2019a; Willemsen et al., 2016). This has been resolved by applying a Smagorinsky factor with a typical value of 0.15 (Pope, 2001). For the horizontal eddy diffusivity, a value of $1 \text{ m}^2/\text{s}$ is implemented which is suitable for the grid size in and around the area of interest (Deltares, 2019a).

Table 1. Overview of input parameters applied within the model.

Parameter	Value	Definition	Source
Domain & time frame			
n	0.021	Manning coefficient	(Zijl et al., 2013)
n_{marsh}	$0.04 \text{ s m}^{-1/3}$	Manning coefficient on the salt marsh	(Wamsley et al., 2010)
C_{bottom}	$0.058 \text{ m}^2 \text{ s}^{-3}$	Jonswap bed friction coefficient	(1)
C_S	0.15	Smagorinsky factor	(Pope, 2001)
K	$1 \text{ m}^2 \text{ s}^{-1}$	Horizontal eddy diffusivity	(Willemsen et al., 2016)
C_{max}	0.7	Maximum courant number	(Deltares, 2019a)
Sediment dynamics			
ρ_{sed}	2650 kg m^{-3}	Specific density sediment	(Deltares, 2019a)
P_{bed}	1600 kg m^{-3}	Dry bed density	(Deltares, 2019a)
D_{50}	$180 \mu\text{m}$	Median grain size	(2)
p_m	0.15 (-)	Mud fraction	(2)
$RWAVE$	1.25 (-)	Calibration factor for wave-related bed-form roughness	(2)

⁽¹⁾ Determined based on calibration of hydrodynamics. ⁽²⁾ Determined based on initial model testing, performed to improve simulated morphological development (Section 2.3.3.1).

Within the model, two different time steps are applied. While the wave module computes wave conditions within an hourly interval, the flow module applies a numerical time step which is based on a maximum Courant number of 0.7. This time step is also applied for morphological computations. Communication between the modules is performed hourly. The first two days were used for morphological spin-up, restricting bed-level change within this period.

In addition, the model will run for two scenarios. The first and standard model includes both the flow and wave modules realistically simulating a month with daily conditions and two storms. The second scenario includes only the flow module, simulating tides with storm surging but excluding wind waves. This will give insight into the significance of wind waves on morphological development.

2.3.2. Hydrodynamics

2.3.2.1. Setup

To derive boundary conditions for the flow module, the Dutch continental shelf model is used (DCSM-FM Model). The DCSM-FM model was developed in-house at Deltares and is able to simulate the effect of tides and storm surges. At the open boundary of the DCSM-FM model, a forcing of the water level is implied using astronomical components. These astronomical components are derived from the tidal model, FES2012 (Carrère et al., 2013). Furthermore, meteorological surface forcing is included, which enables the model to simulate storm surging. This is performed by adding time- and space-varying wind velocities and air pressure (Zijl and Groenenboom, 2019). From this DCSM-FM model, water levels and flow velocities vectors are extracted with a time step of five minutes along the open boundary of the flow domain.

Input for the wave module's boundary condition is estimated, since insufficient data is available along this boundary. The wave heights are estimated based on measured wave heights at the 'Eierlandse Gat boei' (RWS, 2019) and expected wave heights based on observed wind velocities according to (Wright et al., 1999). This results in wave heights along the boundary between 0.5m to 9m occurring with wind velocities between 1 to 23m/s. The wave periods are based on the relation between wave height and period, as determined in (Li et al., 2014). Furthermore, the wave direction is assumed to be equivalent to the wind direction. Since all data used is hourly, the wave-boundary condition has hourly data as well.

Due to the dimensions of both domains, surface forcing is required. For this purpose, data from the 'High Resolution Limited-Area Model' (HiRLAM) is applied which contains hourly wind vectors and air pressure data with a resolution of 11 by 11km (KNMI, 2017). For both the flow- and wave modules, the wind data is applied, which accommodates both the wind velocity and direction. Within the flow module, the air-pressure data is used as well.

2.3.2.2. Calibration

Research indicates that wind waves are an important factor for salt marsh development, both for accretion by sediment supply and for erosion by wave action (Bouma et al., 2016; Schuerch et al., 2019). Therefore, optimisation of wind wave modelling is desirable. This will be performed by calibrating the bed friction coefficient within the wave module for both the Jonswap and Madsen formulation (Hasselmann et al., 1973; Madsen et al., 1991). To determine which bed friction coefficient performs best, the resulting significant wave heights will be compared with observations at the nearest measurement station 'Wierummerwad'. The optimal simulation will be determined based on the Nash Sutcliffe coefficient (NS) (Nash and Sutcliffe, 1970). This coefficient is chosen because high values have a comparatively higher impact, which is also true for erosion by wind waves (Leonardi et al., 2016).

2.3.2.3. Validation

In addition, the simulated hydrodynamics will be validated by comparing the output with observed historical water levels at all available measurement stations within the model domain. For validation of the water levels, this will be performed using the 'index of agreement' (Skill) which focusses on mean

values (Elias et al., 2012; Willmott, 1981). It will also be accomplished with the NS, which focuses on extreme values (Nash and Sutcliffe, 1970). The data will be compared with a five-minute interval. For validation of the water level, the station nearest to the study area has no data available in that month. To validate at this location still, November 2017 is modelled as well. For validation of the wave module, the simulated wave heights will also be compared with observations. This will be performed with the NS and the root mean square error (RMSE). This comparison will be based on hourly data.

2.3.3. Sediment dynamics

2.3.3.1. Setup

Within the model, the bed consists of uniform and homogeneous sand with a single median grain size. The specific- and dry-bed density are 2650 kg/m^3 and 1600 kg/m^3 , respectively, which are the default values in D3D-FM and are in agreement with literature (Flemming and Delafontaine, 2000). For the sediment-transport formulation of Van Rijn (1993), default D3D-FM settings were used as well (Deltares, 2019b). Additionally, a Neumann boundary condition is set for the sediment transport. With this option flow entering the system carries sediment at equilibrium concentration profiles. This effectively limits bed-level change at the open boundaries.

The sediment transport formulation is for non-cohesive sediments, though in reality cohesive sediment is also present within the Wadden Sea (Deltares, 2015a; Zwarts et al., 2004). When an increasing fraction of mud is present in the sediment, the bed gradually approaches a cohesive regime, which leads to altered erosion patterns (Van Ledden et al., 2004). To simulate the presence of cohesive sediment, a mud fraction (p_m) is used. In the model, this is implemented such that

$$\tau_{e,cr} = \tau_{s,cr}(1 + p_m)^\beta \quad (1)$$

where $\tau_{e,cr}$ is the critical bed shear stress for erosion (Pa), $\tau_{s,cr}$ is the critical bed shear stress for sand (Pa), p_m is the mud fraction (-) and β is the empirical constant for critical bed shear stress for erosion (-), which is 3 (van Kessel et al., 2012).

To improve the simulated salt marsh erosion rate, initial model testing is performed. This was performed in comparison to the observed annual erosion rate of the marsh (Section 2.1). Based on this initial model testing, a D_{50} of $180 \mu\text{m}$ and a p_m of 0.15 are determined. These values are within the bandwidth in which they are observed nearby the study area as identified by Deltares (2015a) and Zwarts et al. (2004), respectively. Similarly, the wave-related roughness is lowered from its default setting which is performed by setting the calibration factor hereof ($RWAVE$) at 1.25, which is within the advised range for this calibration factor of 1-3 (Deltares, 2019b).

2.3.3.2. Comparing morphological development

The morphological development simulated with the above mentioned settings is also validated. However, no data is available of sediment transport or bed-level change in the simulated period within the model domain. Therefore, bed-level change will be compared with the observed long-term bed-level data introduced in Section 2.1 and literature on the morphological evolution of salt marshes.

2.3.3.3. Sensitivity analysis

The model's sensitivity towards five different parameters is analysed. This is performed for the median grain size, the mud fraction and the wave-related bed roughness—parameters which were determined for the default model based on initial model testing (Section 2.3.3.1). In addition, the sensitivity of the wave height along the open wave boundary and the bed friction on the salt marsh are analysed as well. An overview of the parameters applied are given in *Table 2*. It should be noted that the table's reference values are not the same as the settings for the default model simulation. In the version of this paper which will be submitted later this year, the default simulation of this analysis will have the same settings.

Sediment characteristics have a direct impact on sediment transport and affect morphological development. These characteristics can thus have a significant impact on the computed bed-level change. Also, sediment characteristics can change significantly within the Wadden Sea area (Dankers et al., 2007). To assess the impact of the median grain size, D_{50} will be set at 120, 150 and 180 μm —values observed in sediment measurements within the Wadden Sea (Deltares, 2015a). In addition, the impact of cohesive sediment is analysed. This is performed by adding a mud fraction of 0%, 10% and 20%, values in agreement with literature (Zwarts et al., 2004).

Also, the wave-related roughness ($k_{s,w}$) is varied since Van Rijn (2000) indicated that the magnitude of sediment transport is sensitive towards this parameter. The value of this parameter is changed indirectly by altering the calibration factor for wave-related roughness (*RWAVE*), which has a linear relation with $k_{s,w}$. Besides the default value of 2, *RWAVE* is set at 1.5 and 2.5 as well.

A boundary condition is applied within the wave module. However, no observed wave data is available along this boundary. A method is formulated to estimate these wave characteristics. The significant wave height along the boundary will be set at 50% and 150% of the estimated values to determine the sensitivity of the model towards this estimated boundary condition.

Furthermore, within the flow module, salt marsh vegetation is represented by an increase in the Manning coefficient on the marsh. The model's sensitivity to the simplified representation of vegetation will be analysed as well. Besides the reference value, a Manning coefficient of $0.021 s m^{-0.5}$ and $0.055 s m^{-0.5}$ will be implemented on the salt marsh to represent no vegetation and dense vegetation, respectively (Wamsley et al., 2010).

*Table 2. Input parameters for the sensitivity analysis for the median grain size (D_{50}), mud fraction (P_M), significant wave height along the wave boundary ($H_{s,BC}$), Manning coefficient (n) and calibration factor for wave-related roughness (*RWAVE*).*

Parameter	Unit	Reference value	Low value	High value
D_{50}	μm	150	120	180
p_m	%	0	10	20

$H_{s,BC}$	%	100	50	150
n	$s\ m^{-\frac{1}{3}}$	0.04	0.021	0.055
$RWAVE$	-	2	1.5	2.5

2.4. Addition of artificial structures

Artificial structures are implemented in the model to analyse their impact on the hydrodynamics and morphological development. They are implemented in both the flow and wave modules. The structures affect the flow such that they simulate energy loss and redirect the flow. Within the wave module, the structures can attenuate waves with a transmission coefficient which is either constant or dependent on the incident wave conditions and the height and form of an artificial structure. Sediment transport and erosion and deposition is only affected indirectly, due to the altered hydrodynamic conditions. Figure 6 visualizes the location of the various structures, and the specific structures implemented are described in brief in Table 3 below.

The structure named *Short* represents a small groyne of 2.5 m *N.A.P.* and reduces wave heights such that it represents a dam with a slope of 1:3/2 (Deltares, 2019a). *Long* represents an extended version of *Short* with the same characteristics.

Sedimentation fields are implemented in combination with the groynes. These sedimentation fields have the specific purpose to reduce flow velocities and attenuate waves on and in front of a salt marsh to stimulate local sedimentation (Dijkema et al., 2013). *Combi Long* is a combination of the long groyne with a configuration of a sedimentation field proposed by local authorities. *Combi Short* is a combination of the short groyne and a sedimentation field with a traditional form representing the structures present in the past (Figure 3). Within the flow module, the artificial structures applied for the sedimentation field have a height of 0.7 m above the initial bed-level, with a maximum height of 1.45 m *N.A.P.* similar to sedimentation fields currently present in the Wadden Sea (Dijkema et al., 2013). The same heights are applied for the implementation of *Combi Short* within the wave module, where the groynes represent a thin sheet. Wave attenuation for the sedimentation field of *Combi Long* is performed with a transmission coefficient of 0.55 (Dao et al., 2018). It should be noted that, due to the resolution of the wave grid, the openings in between groynes of the sedimentation field are not present in the wave module. An overview of the specific input parameters applied for the various structures are available in appendix A.

Table 3. An overview of the artificial structure configurations.

Name	Structure form as referred to in Figure 6	Description
Short	1	A short groyne of 2.5m high.
Long	2	A long groyne of 2.5m high.
Combi Long	2+4	Combination of <i>Long</i> and a proposed sedimentation field
Combi Short	1+3	Combination of <i>Short</i> and a traditional sedimentation field

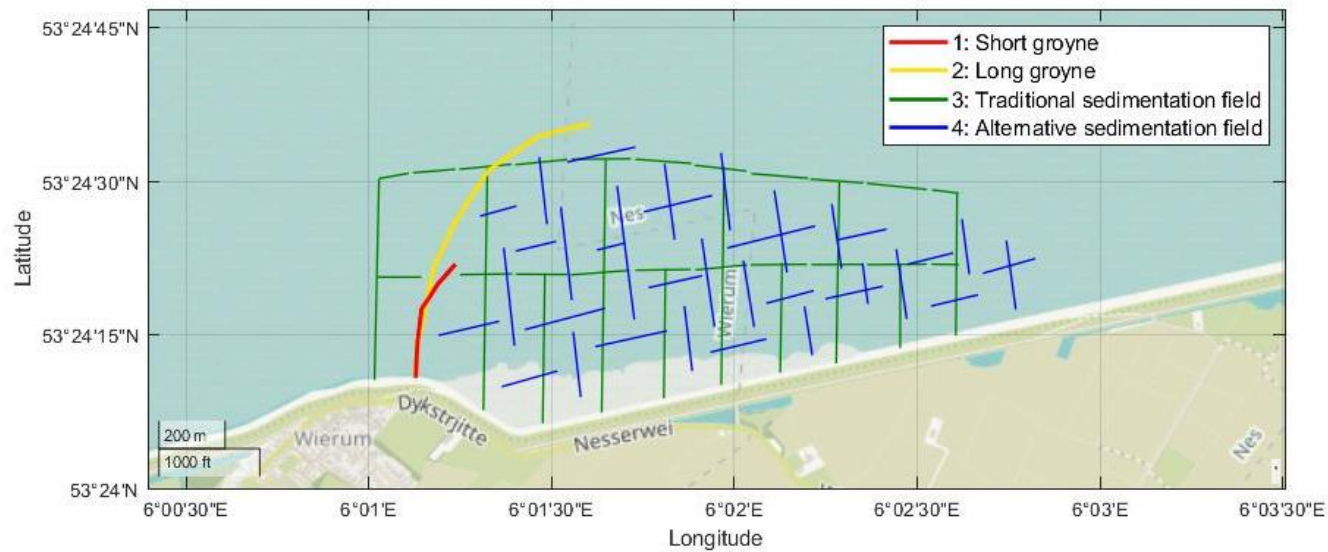


Figure 6. Visualization of the locations and forms of the structures implemented within the model.

3. Results

3.1. Hydrodynamics

To improve simulation of the significant wave heights, calibration is performed for the bed friction coefficient of the wave module. This resulted in a Jonswap bed friction coefficient of $0.058 m^2 s^{-3}$. Subsequently, simulated water levels and the calibrated significant wave heights are validated on all measurement stations with data available. Results showed that the flow module performed good in simulating water levels. The wave module performed well for simulating wave heights. However, the highest wind waves are underestimated. Comparisons of observed and simulated data over time are shown in Appendix A.

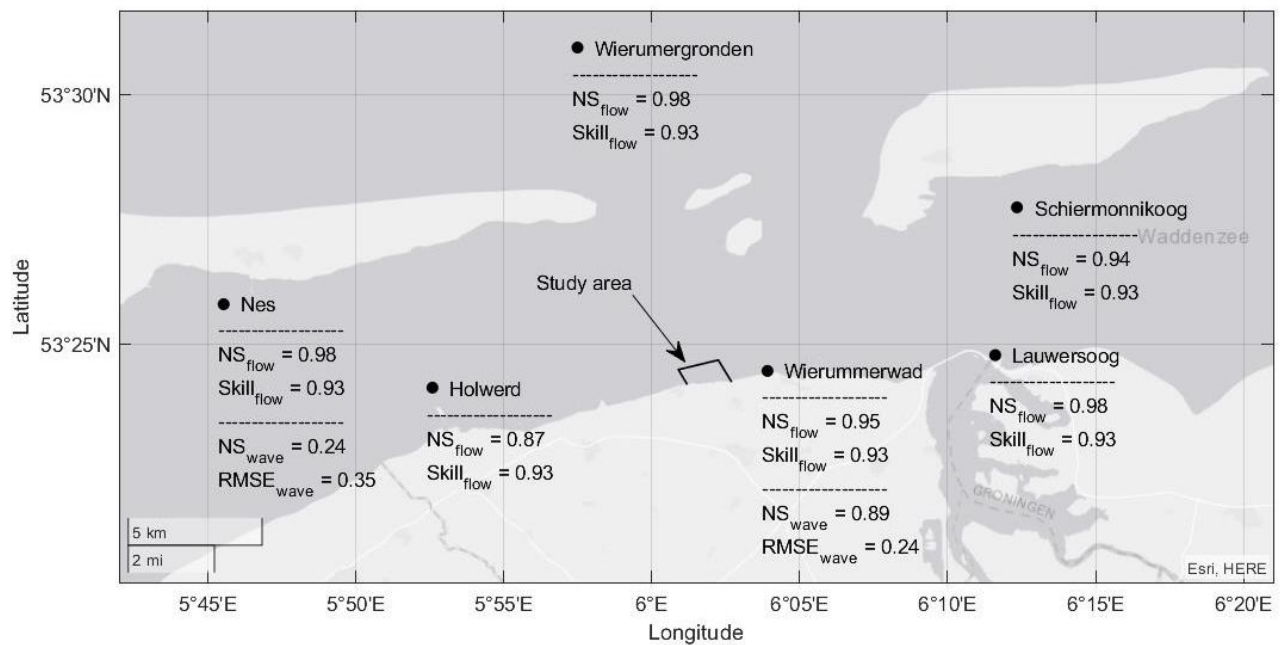


Figure 7. Validation of the hydrodynamics for all measurement stations within the model domain for which data is available. This is performed for the Nash Sutcliffe coefficient (NS) and Index of Agreement (Skill) for validation of the water levels in the flow module (flow). Similarly it is performed for the NS and the Root Mean Square Error (RMSE) for the significant wave heights in the wave module (wave).

3.2. Morphodynamics

3.2.1. Simulated bed-level change

The model scenario in which only the flow module is applied shows that, when wind waves are excluded, all morphological development within the Wadden Sea can be observed in and around the tidal channels, whereas the study area's salt marsh and tidal flat remain almost entirely unchanged.

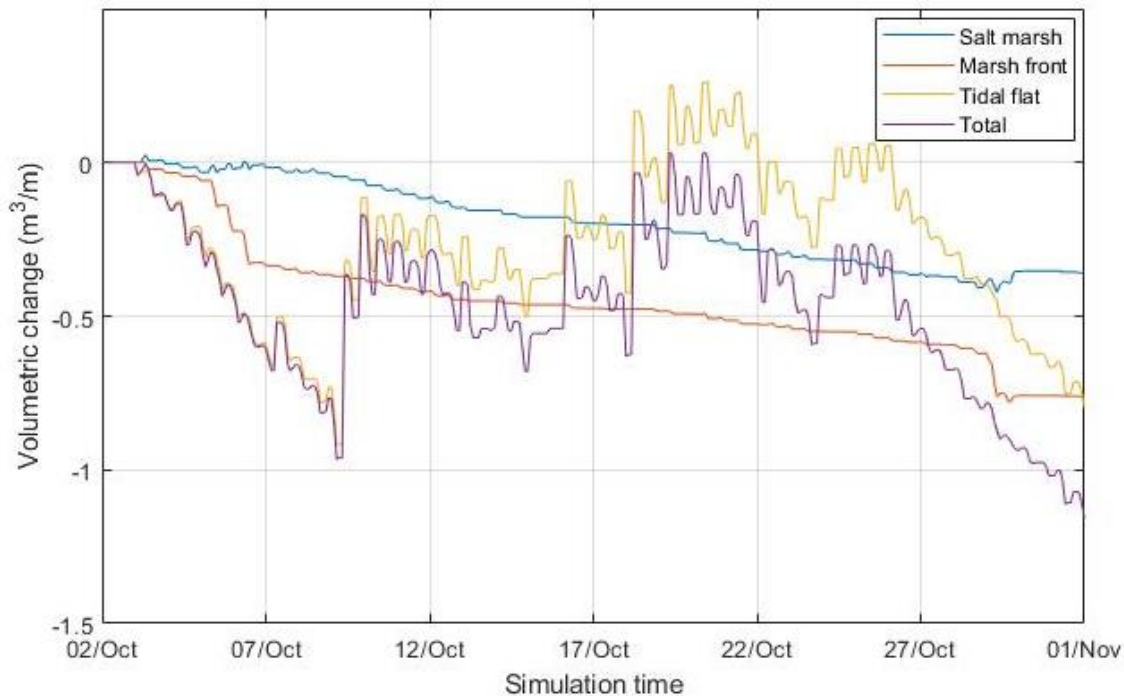


Figure 8. Length averaged volumetric change (m^3/m) over time within the study area.

For the scenario including wind waves, the volumetric change over time within the study area is depicted in Figure 8. Both the tidal flat and salt marsh show, when inundated, erosion during ebb and accretion during flood. The figure also displays a dynamic tidal flat which undergoes both erosion and sedimentation. The salt marsh mostly displays a steady net erosion, almost entirely due to erosion of the marsh front.

Figure 8 also shows that the tidal flat erodes during periods with heavy weather. However, in the middle of the simulated period, when conditions are calmer, the tidal flat exhibits net accretion for several tidal cycles. This accretion is most severe on the tidal cycles of 9 and 19 October. These periods of accretion are paired with a period of flood and low wave heights. The part of the tidal flat close to the marsh undergoes net erosion, while areas with lower bed-levels undergo net accretion (Figure 9). This can be explained by an increasing wave-induced bed shear stress towards the marsh.

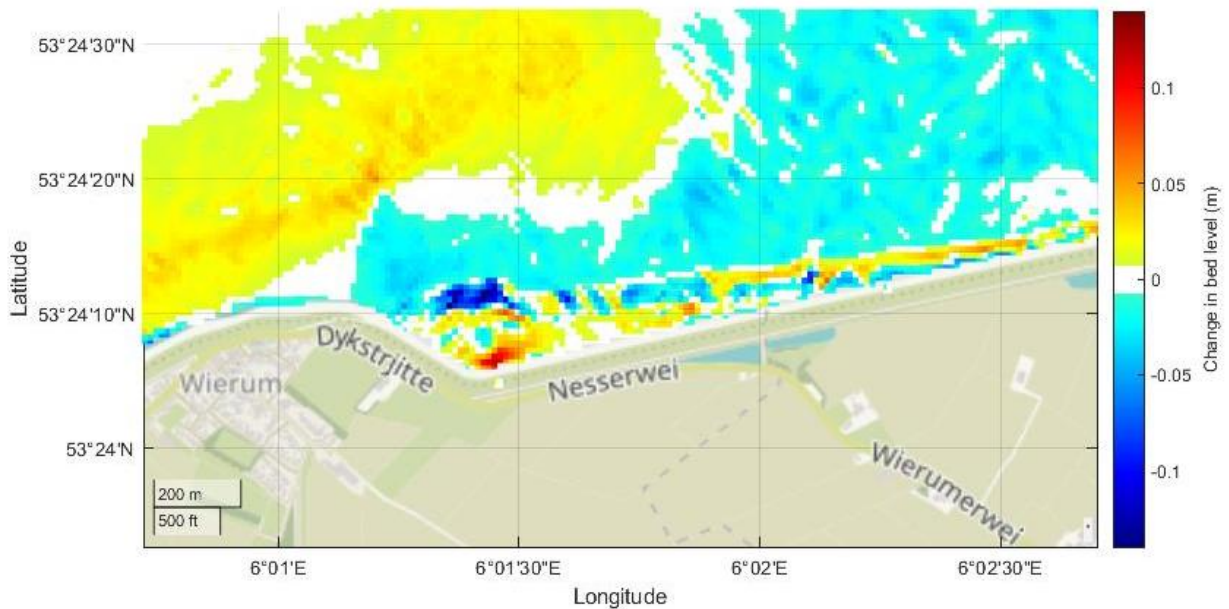


Figure 9. Total simulated bed-level change (m) at the study area in October 2017.

Furthermore, most of the erosion of the salt marsh can be observed along the marsh edge, representing cliff erosion. This erosion occurs along the first 20-50 m of the marsh front. However, as can be observed in Figure 2, realistic cliff erosion occurs only directly adjacent to the marsh edge. This marsh front displays an increased erosion rate during storm periods, when waves are higher (Figure 8). The figure also demonstrates that total erosion of the marsh front is larger than the total salt marsh erosion, as accretion occurs on the marsh when inundated, which is mostly during storms. This accretion is visible in (Figure 9), but also in the observed bed-level data (Figure 2). The total volumetric change on the salt marsh, modelled within the simulated month, is $-0.36 \text{ m}^3/\text{m}$.

3.2.2. Sensitivity analysis

A sensitivity analysis is performed towards five choices made within the model setup. Throughout the sensitivity analysis, spatial erosion and accretion patterns remained fairly similar. The magnitude of erosion or accretion showed large variation. The analysis compares the volumetric change of the salt marsh averaged along its length (m^3/m) at the end of the modelled month. The results hereof are depicted in Figure 10. It should be noted that the default situation in this analysis does not have the same settings as the default model simulation (Table 1, Table 2). In the version of this paper which will be submitted later this year, the default simulation of this analysis will have the same settings.

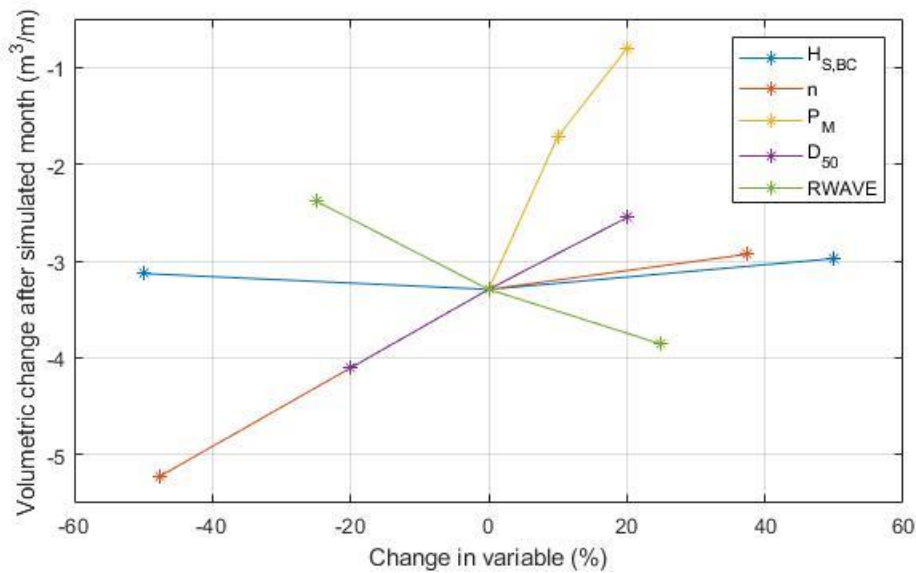


Figure 10. A sensitivity analysis with the length-averaged volumetric change of the salt marsh as indicator. This is performed for the significant wave height along the open boundary ($H_{s,BC}$), the Manning coefficient (n), mud fraction (p_m), median grain size (D_{50}) and calibration factor for wave-related roughness ($RWAVE$).

The figure demonstrates a high sensitivity towards changes to the sediment characteristics and sediment transport formulation. Within the model, a mud fraction is represented by increasing the critical bed shear stress with an inverse relationship. Thus, a mud fraction will lower erosion and potential sediment transport. The addition of 10% mud fraction resulted in a decreased erosion rate of 45%. Similarly, an increased median grain size also increases the critical bed shear stress, but with a linear relationship. In addition, a larger grain size increases the reference sediment concentration as well. This partially compensates for the reduced sediment transport caused by the higher critical bed-shear stress. A similar model sensitivity as for D_{50} is observed for the calibration factor $RWAVE$. As a consequence of reducing this calibration factor, bed shear stresses induced by waves are reduced. This limits erosion due to wind waves. Sediment transport due to flow is not directly affected.

Altering the significant wave height along the wave boundary generates little impact on the volumetric change. The reason behind this is the limited impact of this change on wave heights within the study area. This indicates that local waves within the Wadden Sea are mostly generated by local wind, and not by waves coming from the North Sea. However, it should be noted that wave conditions on the North Sea are affected and thus might not be simulated well.

Furthermore, the model displays a high sensitivity towards a decreased bed roughness on the salt marsh. This change increases local flow velocities and local erosion rates. The results illustrate that an increased bed roughness due to the presence of vegetation result in a more stable bed. Furthermore, the increase in bed roughness from the reference situation shows little impact, indicating a reduced impact when vegetation densities further increase.

3.3. Impact of artificial structures

Within the default model, artificial structures are implemented. The structures named *Base* and *Long* cause set-up of the water level on the wind side and set-down on the lee side. Additionally, they attenuate waves and reduce flow velocities on their lee-side. The short groyne shows little impact towards the hydrodynamics within the study area (*Table 4*), since its area of effect is fairly small. The longer groyne affects a larger area and reduces waves and flow velocities to a larger degree, resulting in lower mean flow velocities and wave heights within the study area. However, the effectiveness of both groynes to attenuate waves depends on wind directions. Where the structures impact is most significant when waves come from a western direction, its impact is reduced during the simulated storms when wind directions are north to north-west.

Table 4. Comparison of hydrodynamics within the whole study area for the configurations of artificial structures. Based on data with a two hour interval.

Simulation	Mean flow velocity (cm/s)			Mean wave height (cm)		
	Storm	Calm	Total	Storm	Calm	Total
Default	18.7	8.2	10.3	20.5	3.0	6.2
Short	17.5	7.9	9.9	19.9	2.8	5.9
Long	11.3	6.4	7.5	17.6	2.3	5.1
Combi Long	10.3	6.3	7.1	14.7	2.1	4.4
Combi Short	12.9	5.5	6.8	9.7	0.6	2.6

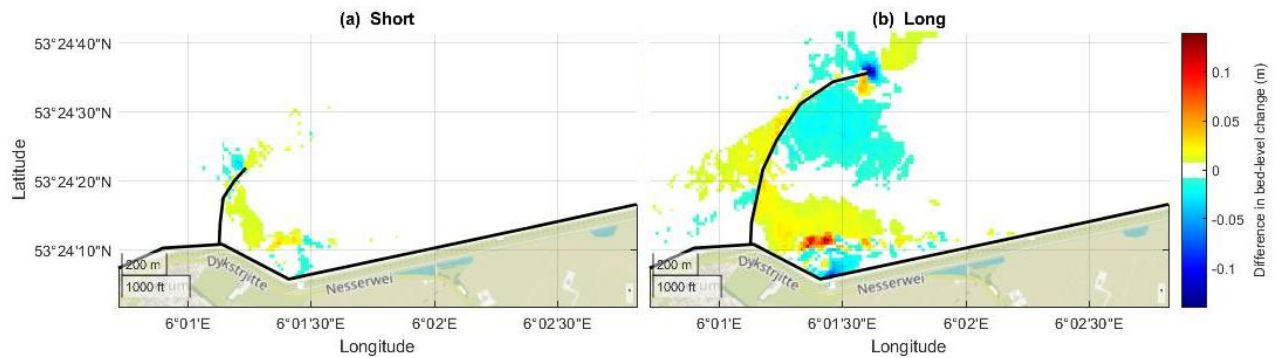


Figure 11. Difference in simulated bed-level change compared to the default model for the structures (a) Short and (b) Long. Hard structures in the simulation are displayed by black lines.

Due to the changes in hydrodynamic conditions caused by the artificial structures, morphological development is altered. The reduced wave heights and flow velocities reduce local bed shear stresses and thus erosion rates. In addition, sediment in the water column has more time to settle due to reduced flow velocities (Deltares, 2019b). The differences in bed-level change, relative to the default model, are depicted in *Figure 11*. The figure illustrates that both groynes reduce erosion of the marsh front. Accretion on the marsh is reduced as well due to reduced sediment supply towards the marsh. Erosion on the tidal flat directly in front of the marsh is reduced. However, the long groyne also causes net erosion further seawards. This is caused by the structure blocking alongshore sediment transport. Because of this, net accretion during the calm period is reduced in the simulation with the long groyne,

while the short groyne increases net accretion during this period (Figure 13.c). In addition, holes and depositional lobes develop at the tip of the groynes due to increased local flow velocities (Figure 12).

For *Combi Long* and *Combi Short*, sedimentation fields are added to the groynes. Within *Combi Long*, the long groyne is present, which limits sediment supply to the study area. Due to the addition of the sedimentation fields to the long groyne, wave heights are further reduced (Table 4) which further reduces erosion of the marsh edge and sediment supply towards the marsh (Figure 13.a-b). On the tidal flat, compared to the long groyne, the sedimentation field generally reduces local flow velocities during storms, while flow velocities remain similar during the calm period (Table 4). Consequently, net erosion on the tidal flat during storms is decreases, while net erosion during calm periods increases (Figure 13.c).

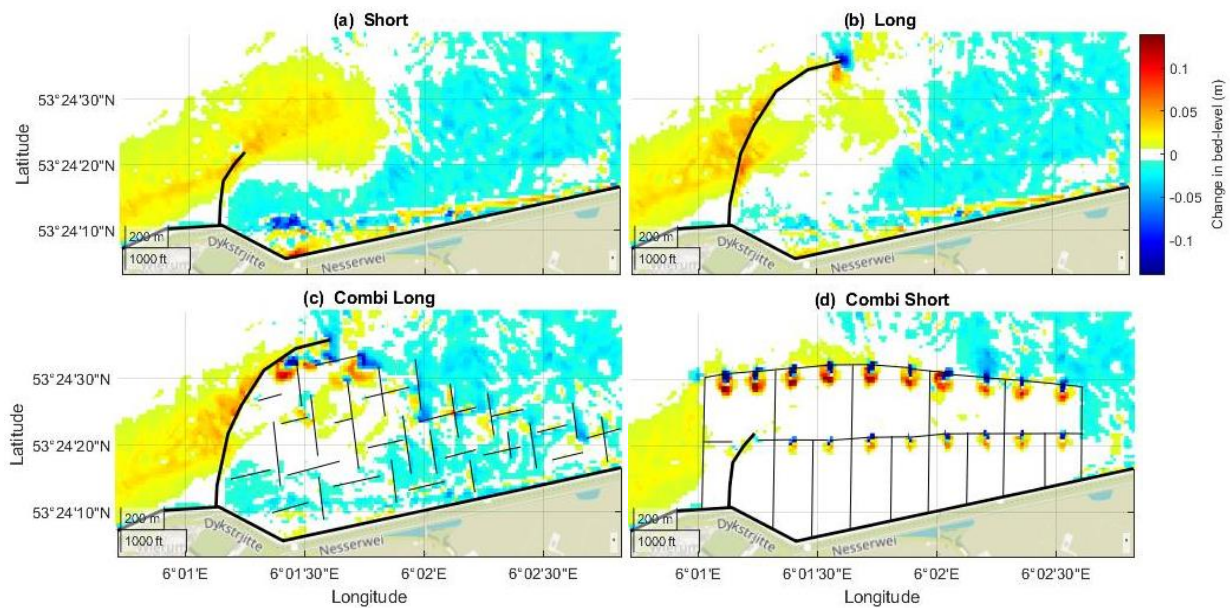


Figure 12. Simulated change in bed-level within the study area for the structures (a) Short, (b) Long, (c) *Combi Long* and (d) *Combi Short*. Hard structures in the simulation are depicted by black lines.

The artificial structures used for *Combi Short* show a large impact for the whole study area. The sedimentation field reduces wave heights to a larger degree than *Combi Short*. Furthermore, the sedimentation field generates a constant attenuation of the flow velocity, both during calm weather and storms (Table 4), further reducing bed shear stresses and increasing potential for sediment to settle. As a result, erosion on the tidal flat during storms is significantly reduced and sedimentation is observed during the calm period resulting in net accretion for the whole simulated period (Figure 13.c). In addition, the salt marsh remains almost unchanged, both on the marsh front due to wave attenuation, and on the marsh itself since sediment supply to the marsh is limited. Similarly to *Long*, the structures still block alongshore sediment transport limiting sediment supply to the study area.

Outside of the study area, all structures cause reduced erosion on the lee-side. On the wind side accretion is reduced. This effect is stretched out over 1km along the coast on both sides and no differences larger than 1 cm are observed relative to the default model (*Figure 11*).

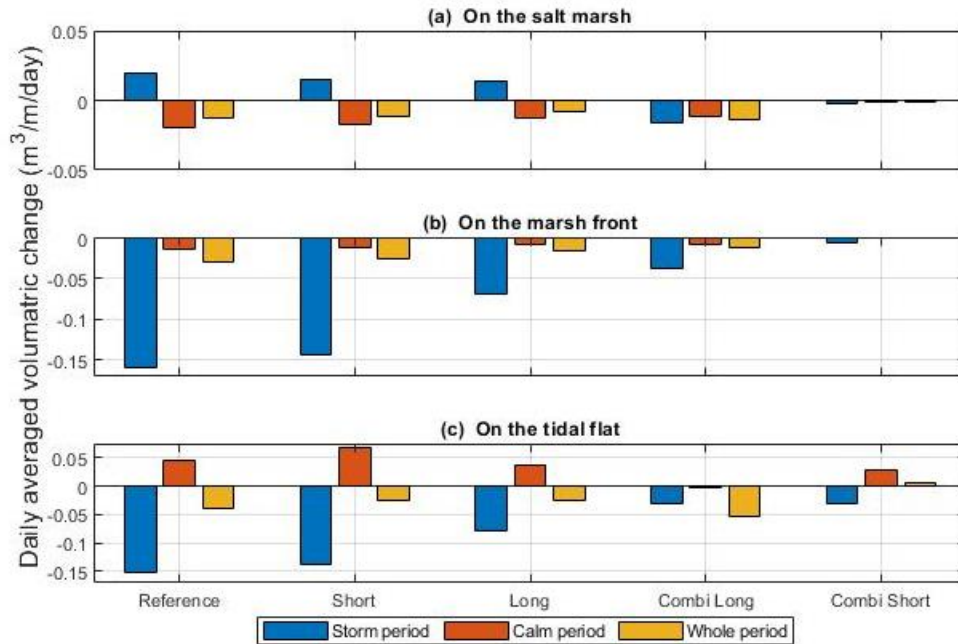


Figure 13. Daily and length averaged volumetric change (a) on the salt marsh, (b) on the salt marsh front and (c) on the tidal flat. The storm period is the combined bed-level change for the storms of 4-5 October and 27-28 October. The calm period is from 8 to 21 October. The whole period is for the whole simulated month.

4. Discussion

This paper reports on the first research application of the Delft3D Flexible Mesh modelling software applying a coupled flow-wave module and morphodynamics to simulate salt marsh development. The model applies both boundary and surface forcing to successfully simulate daily conditions and storm conditions. Based on the hydrodynamic forcing, bed-level change on and around an eroding salt marsh are simulated. With the combination of surface forcing and a flexible mesh, we are able to study both small- and large-scale morphological processes within the same simulation while computation times can be kept relatively low (6 days for 1 computational core). In addition, structures are implemented within the model, providing the possibility to assess the impact of human interventions on salt marsh dynamics.

4.1. Assumptions and uncertainties

The model was run in 2DH, as solving the equations in 3D showed similar results but significantly increased computation time (Horstman et al., 2015; Willemsen et al., 2018).

Surface forcing is simulated based on HiRLAM data, which has a resolution of 11 by 11km. Since the barrier islands of the Wadden Sea are of similar dimensions, the impact of those islands to the wind velocities and directions are probably not considered well. Consequently, wave generation by wind on the lee-side of the barrier islands may be overestimated. In addition, the sensitivity analysis of the wave boundary condition indicates that wind waves within the study area are almost entirely dependent on the surface forcing, which is supported by literature as well (Oost, 1995). This shows the importance of proper surface forcing data within the Wadden Sea. However, wave heights are calibrated for local conditions, and the influence of overestimating wind velocities will thus be compensated for within the study area.

Within the flow module, vegetation is represented by applying an increased bed roughness on the salt marsh. This effectively reduces erosion rates on the marsh. The ability of vegetation to function as sediment trap is hereby not considered, nor is the wave attenuating ability of the vegetation. However, salt marsh growth initiates with accretion of the tidal flat. Since no vegetation will be present on the tidal flat within the simulated period, the simplified implementation of vegetation will not directly affect the analysis of salt marsh growth. It will however, reduce accretion and increase wave heights on the marsh itself.

While water levels and wave heights are validated, the flow directions and velocities and wave directions are not validated since no observed data is available hereof. While the flow velocity affects the magnitude of sediment transport, sediment transport directions are derived from the flow and wave directions. These hydrodynamic properties are the main form of uncertainty in the simulated hydrodynamics.

The sediment transport formulation of van Rijn (1993) is applied to derive morphological development based on the hydrodynamic conditions. This formulation has reduced accuracy for bed material with $D_{50} < 200 \mu m$. In addition, the magnitude of sediment transport is sensitive towards wave-related bed-form roughness, an input parameter of which little data is available (Van Rijn, 2000). Also, the model shows high sensitivity towards varying D_{50} and p_m , input parameters of which no accurate data is available. Because of the models sensitivity towards these input parameters, the magnitude of sediment transport, and thus erosion and accretion rates, contain large uncertainty.

The applied sediment transport formulation is for non-cohesive sediments only. However, in reality cohesive sediment is present as well (Zwarts et al., 2004). The lowered erosive characteristics when cohesive sediment is present is represented with a mud fraction. However, actual transport of cohesive sediment is not implemented, though this transport can lead to altered morphological patterns (Van Ledden et al., 2004). Most notably, mud moves —to a larger extend than sand— to areas with lower energy such as a tidal flat and salt marsh (Friedrichs, 2011). The addition of mud transport is thus likely to result in more sediment deposition in the higher regions of the study area. However, in the setup of the model, settings were chosen such that the simulation of morphological development was improved (section 2.3.3.1). Hereby, the absence of cohesive sediment may partially be compensated for.

Within the sensitivity analysis, differences in bed-level change occurred mostly in the rate of erosion or accretion. Spatial morphological patterns remained similar throughout. Moreover, the model captures several key morphological processes, such as accretion of the tidal flat and salt marsh during flood and erosion hereof during ebb, sediment supply due to wave stirring and a retreat of the marsh edge due to wave attacks. This demonstrates the robustness of the simulated morphological patterns.

4.2. Default simulation

Validation of the hydrodynamic conditions is performed for both the water levels and wave heights. While water levels are generally modelled well, differences are observed at low water levels at some measurement stations. This is caused by differences in bed-level, since the local bathymetry originates from 2012 while the model simulates a period in 2017. The significant wave heights were simulated reasonably well. However, low wave heights were underestimated which is most likely also caused by the differences in bed-level. High waves are underestimated as well, which may be caused by a wave-breaking parameter which is too low (Appendix A).

Validation of the simulated morphological development is performed by comparing it with the observed long-term morphological development. Besides that, several morphological processes are identified in literature as well. For instance, results indicate that almost all morphological development on the tidal flat and salt marsh occur due to wind waves. This is supported by literature, which indicates that wind waves are directly related to both sediment supply and erosion rates for salt marshes (Best et al., 2018; Leonardi et al., 2016). In addition, both the tidal flat and salt marsh show, when inundated, erosion during ebb and accretion during flood (*Figure 8*). This is supported by basic theory on salt marsh evolution (Loon-Steensma, Slim, et al., 2012). *Figure 8* also demonstrates a dynamic tidal flat next to a

relatively stable marsh, which is observed by Willemsen et al. (2018). At the marsh front, an increased erosion rate is observed during storm periods, when waves are higher, which is supported by theory on salt marsh cliff erosion (Leonardi et al., 2016). During these storms, accretion on the salt marsh is observed. This process is identified in literature as well, where Oost (1995) reports up to several decimetres of accretion after a storm.

Observed bed-level data exhibited annual volumetric change averaged along the length of the salt marsh of $-1.1 \text{ m}^3/\text{m}/\text{year}$ (Figure 2). Applying the same method of data analysis for the simulation exhibits a volumetric change of $-0.36 \text{ m}^3/\text{m}/\text{month}$ (Figure 8). Morphological development of a marsh mainly occurs within the period of October till February (Oost, 1995). Assuming all bed-level change on a marsh occurs within these 5 months, and erosion during those months are equal, results in a estimated simulated erosion of $1.8 \text{ m}^3/\text{m}/\text{year}$. This is an overestimation of 64%. One could argue that two storms are present within the simulated month with water levels and wind speeds which have a reoccurrence of 1.5 times (RWS, 2019) and 1 time per year (KNMI, 2019), respectively. Consequently, erosion rates within the simulated month will be higher. However, during the storms slight accretion is simulated on the salt marsh (Figure 8), refuting this argument. While storms do not substantially increase net erosion of the marsh, the storms do increase erosion of the salt marsh front. Therefore, large erosion rates are simulated here.

Salt marsh growth is initiated by accretion of the tidal flat. The observed bed-level data already shows accretion of the tidal flat (Figure 2), which suggests that the study area has potential for salt marsh growth. In the simulation, that same area shows net erosion (Figure 9). The cause hereof is the heavy weather that is simulated, since accretion is simulated during relatively calm weather (Figure 8) indicating that the potential for marsh growth is present in the simulation as well.

The simulated erosion along the marsh front occurs due to wave energy, similar to realistic erosion of a marsh cliff (Bouma et al., 2016). However, the model does not simulate a retreating marsh due to actual cliff erosion as displayed in the observed data (Figure 2) since simulated erosion of the marsh occurs along 20-50m of the marsh width (Figure 9). The width of the marsh front experiencing erosion can be reduced by increasing the grid resolution and introducing an increased cohesiveness at the top layer of the marsh, representing the cohesive and vegetated top layer of a marsh (Francalanci et al., 2013). However, the processes required to accurately describe cliff erosion are not part of D3D-FM (Deltares, 2019b).

4.3. Artificial structures

The results with artificial structures indicate that, while the groynes are able to reduce energy within the study area, sedimentation fields show larger potential to steer morphological development of the marsh and tidal flat. Not only are the sedimentation fields less dependent on the direction of wind waves to be effective, they are also able to consistently and considerably reduce flow velocities (Table 4).

The potential of sedimentation fields to steer salt marsh development is most notably in *Combi Short*. Both flow velocities and wave heights are substantially reduced due to the addition of the

sedimentation field to the short groyne (Table 4). As a consequence hereof, erosion is minimal during the entire simulated period (Figure 13). In addition, on the tidal flat *Combi Short* is the only configuration which results in net accretion for the whole period (Figure 8).

In *Combi Long*, the addition of a sedimentation field to the long groyne does not reduce flow velocities and wave heights to such an extent as due to the traditional sedimentation field of *Combi Short* (Table 4). Moreover, the impact of *Combi Long* on bed-level change is not as substantial as for *Combi Short* (Figure 13), though the structures implemented for these sedimentation fields have a similar total length. This indicates that, while sedimentation fields can have a large impact, a proper configuration of the structure should be implemented to be effective and efficient.

While results with *Combi Short* indicates the potential for stimulating salt marsh growth by implementing a traditional sedimentation field, such a configuration is not necessarily the desired structure for ecology or policy. The sedimentation field has the most impact on local flow conditions, implicating that the impact on its surrounding is likely also most severe. Since the study area is located in the Wadden Sea, an area protected by Natura 2000, radical changes to the natural systems may not be expedient. If it is desired to stabilize an eroding marsh and impact on its surroundings should be minimal, a small intervention may suffice.

Four different morphological developments of salt marshes or tidal flats are identified which are likely the crucial indicators for policy makers when steering salt marsh development. In TABLE 5, the artificial structures are ranked on how well they performed in steering these specific morphological developments. Results indicate that accretion of the marsh and erosion of the marsh front have a negative relationship. Namely, wave attenuation results in reduced erosion of the marsh front. However, less sediment is transported onto the marsh as well, reducing marsh accretion. To assess which structure performs best to stimulating salt marsh growth, accretion of the tidal flat is the crucial indicator when a tidal flat is not sufficiently high —relative to the water level— for vegetation to establish. When a tidal flat has sufficiently accreted for vegetation establishment the stability of the tidal flat is of key importance, since large perturbation of the bed-level will cause burying or toppling of pioneer vegetation (Hu et al., 2015).

TABLE 5. QUALITATIVE RANKING OF HOW WELL THE ARTIFICIAL STRUCTURES CAN STEER MORPHOLOGICAL DEVELOPMENT.

	Base 1	Long 1	Combi Long	Combi Short
Allowing accretion salt marsh	1	2	3	4
Reduced erosion marsh front	4	3	2	1
Accretion tidal flat	3	2	4	1
Stability tidal flat	4	3	2	1

It should be considered that the impact of structures are assessed for an eroding marsh. When a salt marsh is healthy, and no cliff erosion occurs, the same analysis may provide different results. In addition, although the results show clear erosion and accretion trends, only the initial impact after

structure implementation is modelled. The impact of the structures and of initial bed-level changes on long-term morphological development is still missing. Similarly, outside of the study area little differences in bed-level change were observed due to structures implemented. However, this may not be so when a longer time period is simulated. Furthermore, permeable structures could not be implemented within the model. Since results indicate that the restriction of flow has both pros and cons, by reducing flow velocities but blocking alongshore sediment transport as well, permeable groynes may prove to an effective tool for steering salt marsh development.

4.4. General applicability

Within this paper, morphological development of a salt marsh is simulated. The methods described in Section 2.3 can be applied to create a similar model focussing on other salt marshes. This can be within the Wadden Sea, or more widely, within the area encompassed within the DCSM-FM model, since the used surface forcing from the HiRLAM dataset covers this area as well. The model setup can be adapted such that it can be used for long-term modelling as well. However, the simplified implementation of vegetation will not suffice since vegetation establishment is not being accounted for (Hu et al., 2015).

Results show that there is potential for salt marsh growth within the study area. Not only does the tidal flat already show slight accretion (*Figure 2*), the implemented structures and most notably *Combi Short*, are able to reduce salt marsh erosion and stimulate its growth by increasing accretion on the tidal flat (*Figure 13*).

More broadly, the simulations show that the salt marsh accretes during storm events (*Figure 13*). This demonstrates that salt marsh systems may provide a resilient supplement to hard structures to improve coastal safety in the face of the increasing storminess (Woth et al., 2006).

Moreover, results with artificial structures indicate that morphological development of a salt marsh can be steered by implementing various structures. Groynes can reduce erosion rates of the marsh front and are able to increase accretion of the tidal flat during calm weather. However, their potential impact on morphological development is not as substantial as sedimentation fields. These sedimentation fields have the potential to further reduce marsh erosion and cause accretion on the tidal flat in front of the entire salt marsh, proving to be a viable tool for stimulating salt marsh growth.

5. Conclusion

This paper shows how engineering solutions can be applied to steer the morphological development of salt marshes. This is performed with a morphological model (Delft3D FM) which was setup for an eroding marsh. Daily conditions and two storms with a reoccurrence of 1-1.5 times annually were simulated. Additionally, engineering structures were implemented to analyse how they affect the morphological development.

In the model, hydrodynamic conditions were simulated well. Key processes relevant for the morphological development of salt marshes were captured within the simulation. Groynes and sedimentation fields were implemented in the study area. Simulations showed the potential for salt marsh growth within the study area. More broadly, results demonstrated that salt marshes can be a resilient supplement for coastal safety in the face of increasing storminess. Furthermore, simulations indicated the potential to stimulate salt marsh growth with sedimentation fields. Compared to groynes, these sedimentation fields are less dependent on wind direction to attenuation waves. In addition, they are able to consistently and considerably reduce flow velocities, both on the salt marsh and tidal flat. Due to the implementation of a sedimentation field, net sedimentation was simulated on the tidal flat which can lead to salt marsh growth over time.

It should be considered that the model demonstrates how the study area is affected directly after structure implementation (1 month). However, morphological processes often occur on a time scale of years or decades. Future research on the impact of structures on long-term morphological development is advised.

Appendix

A Validation of hydrodynamics

A.1. Flow module

In *Figure 14* below, the observed and modelled water levels at measurement station ‘Lauwersoog’ are shown. The figure displays that the model performs well for both the extreme and mean water levels.

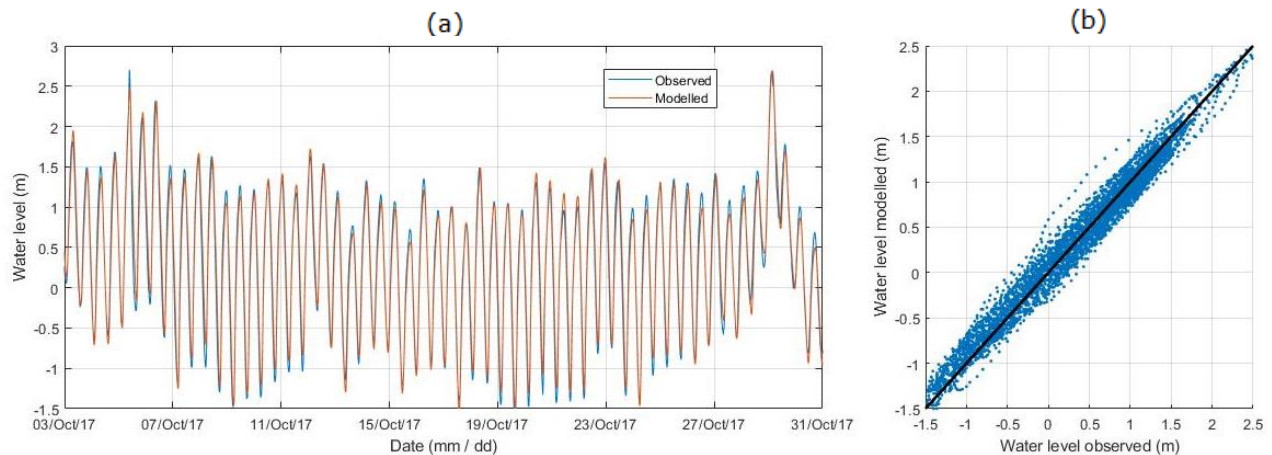


Figure 14. Comparison of observed and modelled water levels at measurement station ‘Lauwersoog’ (a) over time and (b) in a scatter plot where the black line indicates a perfect simulation.

A.2. Wave module

The wave module is calibrated and subsequently validated as well on the significant wave height. The calibration, with an optimization for the NS, resulted in a Jonswap bed friction coefficient of $0.058 \text{ m}^2 \text{ s}^{-3}$. A comparison of the wave heights for an advised Jonswap bed friction coefficient of $0.038 \text{ m}^2 \text{ s}^{-3}$ (Zijlema et al., 2012) and the optimal value is displayed for the measurement station ‘Wierummerwad’ in *Figure 15*. Although the peak wave height is simulated less accurately with the optimized bed friction, the model exhibits improved performance for the lower wave heights, thereby resulting in an improved NS.

The model performs well for the measurement station ‘Wierummerwad’. In general, it underestimates extreme values, and mid-range values are overestimated. At measurement station ‘Nes’, the high waves are simulated worse compared to station ‘Wierummerwad’, while low- and mid-range values are modelled similarly.

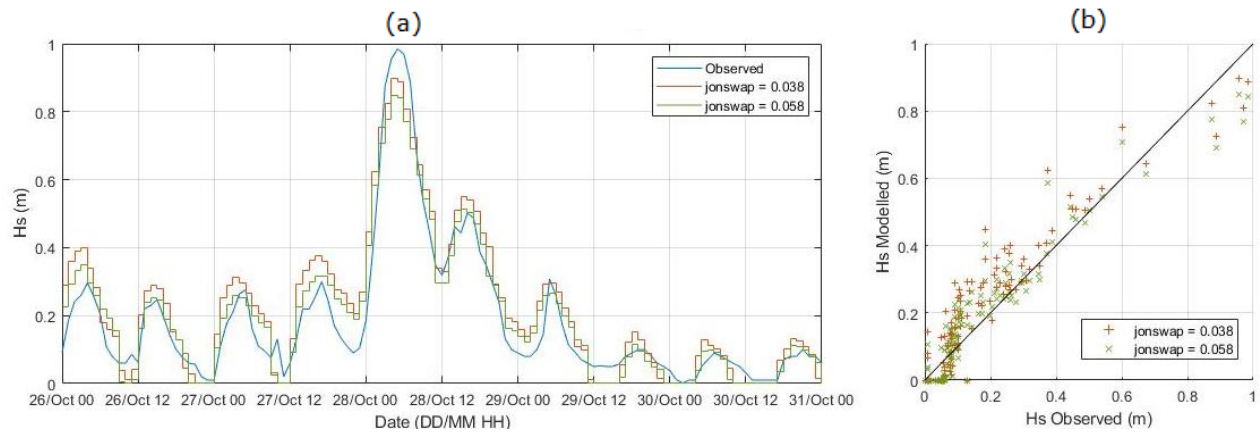


Figure 15. Comparison of observed and modelled significant wave heights with the advised and calibrated bed friction at measurement station 'Wierummerwad' (a) over time and (b) in a scatter plot where the black line indicates a perfect simulation.

B. Input parameters structure implementation

Parameter	Value	Definition	Module	Source
Short; Long				
H	2.5 m	Height structure	Flow	(1)
H_D	2.5 m	Dam height	Wave	(1)
α_D	2.6 (-)	Alpha of dam	Wave	(Deltares, 2019a)
B_D	0.15 (-)	Beta of dam	Wave	(Deltares, 2019a)
Combi Long				
H	Max 0.75 m above bed-level -or- 1.45 m N.A.P.	Height structure	Flow	(Dijkema et al., 2013)
K_{bg}	0.55 (-)	Transmission coefficient of brushwood groyne	Wave	(Dao et al., 2018)
Combi Short				
H	Max 0.75 m above bed-level -or- 1.45 m N.A.P.	Height structure	Flow	(Dijkema et al., 2013)
α_G	1.8 (-)	Alpha of brushwood groyne	Wave	(Deltares, 2019a)
B_G	0.10 (-)	Beta of brushwood groyne	Wave	(Deltares, 2019a)

⁽¹⁾ Equal to other groynes in the Wadden Sea (AHN, 2014).

References

- AHN. (2014). *Actueel Hoogtebestand Nederland (AHN)*.
- Best, U. S. N., Van der Wegen, M., Dijkstra, J., Willemssen, P. W. J. M., Borsje, B. W., & Roelvink, D. J. A. (2018). Do salt marshes survive sea level rise? Modelling wave action, morphodynamics and vegetation dynamics. *Environmental Modelling & Software*, *109*, 152-166. doi:10.1016/j.envsoft.2018.08.004
- Booij, N., Ris, R. C., & Holthuijsen, L. H. (1999). A third - generation wave model for coastal regions: 1. Model description and validation. *Journal of geophysical research: Oceans*, *104*(C4), 7649-7666.
- Bouma, T. J., van Belzen, J., Balke, T., van Dalen, J., Klaassen, P., Hartog, A. M., . . . Herman, P. M. J. (2016). Short-term mudflat dynamics drive long-term cyclic salt marsh dynamics. *Limnology and Oceanography*, *61*(6), 2261-2275. doi:10.1002/lno.10374
- Carrère, L., Lyard, F., Cancet, M., Guillot, A., & Roblou, L. (2013). *FES 2012: a new global tidal model taking advantage of nearly 20 years of altimetry*. Paper presented at the 20 Years of Progress in Radar Altimetry.
- Chang, E. R., Veeneklaas, R. M., Bakker, J. P., Daniels, P., & Esselink, P. (2016). What factors determined restoration success of a salt marsh ten years after de - embankment? *Applied Vegetation Science*, *19*(1), 66-77.
- Charnock, H. (1955). Wind stress on a water surface. *Quarterly Journal of the Royal Meteorological Society*, *81*(350), 639-640.
- Chmura, G. L., Anisfeld, S. C., Cahoon, D. R., & Lynch, J. C. (2003). Global carbon sequestration in tidal, saline wetland soils. *Global biogeochemical cycles*, *17*(4).
- Costanza, R., d'Arge, R., de Groot, R., Farber, S., Grasso, M., Hannon, B., . . . van den Belt, M. (1997). The value of the world's ecosystem services and natural capital. *Nature*, *387*(6630), 253-260. doi:10.1038/387253a0
- Dankers, N., Cremer, J., Dijkman, E., Brasseur, S., Dijkema, K., Fey-Hofstede, F., . . . Smit, C. (2007). *Ecologische Atlas Waddenzee: IMARES*.
- Dao, T., Stive, M. J., Hofland, B., & Mai, T. (2018). Wave Damping due to Wooden Fences along Mangrove Coasts. *Journal of Coastal Research*, *34*(6), 1317-1327.
- Deltares. (2015a). *Dataset: Sediment atlas wadden sea*.
- Deltares. (2015b). *Dataset: Vaklodingen*.
- Deltares. (2019a). Delft3D FM Suite; D-Flow manual.
- Deltares. (2019b). Delft3D FM Suite; D-Morphology manual.
- Dijkema, K. S., van Duin, W., Dijkman, E., Nicolai, A., Jongerius, H., Keegstra, H., & Jongsma, J. J. (2013). *Friese en Groninger kwelderwerken : monitoring en beheer 1960-2010*.
- Elias, E. P., Gelfenbaum, G., & Van der Westhuysen, A. J. (2012). Validation of a coupled wave - flow model in a high - energy setting: The mouth of the Columbia River. *117*(C9).
- Flemming, B., & Delafontaine, M. (2000). Mass physical properties of muddy intertidal sediments: some applications, misapplications and non-applications. *Continental Shelf Research*, *20*(10-11), 1179-1197.
- Francalanci, S., Bondoni, M., Rinaldi, M., & Solari, L. (2013). Ecomorphodynamic evolution of salt marshes: Experimental observations of bank retreat processes. *Geomorphology*, *195*, 53-65.
- Friedrichs, C. (2011). 3.06 Tidal Flat Morphodynamics: A Synthesis.
- Haff, P. K. (1996). *14 Limitations on Predictive Modeling in Geomorphology*. Paper presented at the The Scientific Nature of Geomorphology: Proceedings of the 27th Binghamton Symposium in Geomorphology, Held 27-29 September, 1996.
- Hasselmann, K., Barnett, T., Bouws, E., Carlson, H., Cartwright, D., Enke, K., . . . Kruseman, P. (1973). Measurements of wind-wave growth and swell decay during the Joint North Sea Wave Project (JONSWAP). *Ergänzungsheft 8-12*.
- Horstman, E. M., Dohmen-Janssen, C. M., Bouma, T. J., & Hulscher, S. J. (2015). Tidal-scale flow routing and sedimentation in mangrove forests: Combining field data and numerical modelling. *Geomorphology*, *228*, 244-262.
- Hu, Z., van Belzen, J., van der Wal, D., Balke, T., Wang, Z. B., Stive, M., & Bouma, T. J. (2015). Windows of opportunity for salt marsh vegetation establishment on bare tidal flats: The

- importance of temporal and spatial variability in hydrodynamic forcing. *Journal of Geophysical Research-Biogeosciences*, 120(7), 1450-1469. doi:10.1002/2014jg002870
- KNMI. (2017). *KNMI HiRLAM Data Package*. Retrieved from: data.overheid.nl/dataset
- KNMI. (2019). *Klimatologie*. Retrieved from: projects.knmi.nl/klimatologie/uurgegevens
- Leonardi, N., Ganju, N. K., & Fagherazzi, S. (2016). A linear relationship between wave power and erosion determines salt-marsh resilience to violent storms and hurricanes. *Proceedings of the National Academy of Sciences*, 113(1), 64-68.
- Li, F., Van Gelder, P., Ranasinghe, R., Callaghan, D., & Jongejan, R. (2014). Probabilistic modelling of extreme storms along the Dutch coast. 86, 1-13.
- Loon-Steensma, J. M., Groot, A. V., Duin, W. E., Wesenbeeck, B. K., & Smale, A. J. (2012). Zoekkaart Kwelders en Waterveiligheid Waddengebied. *Alterra-rapport 2391*
- Loon-Steensma, J. M., Slim, P. A., Vroom, J., Stapel, J., & Oost, A. P. (2012). Een Dijk van een Kwelder; Een verkenning naar de golfreducerende werking van kwelders.
- Madsen, O. S., Mathisen, P. P., & Rosengaus, M. M. (1991). Movable bed friction factors for spectral waves. In *Coastal Engineering 1990* (pp. 420-429).
- Millard, K., Redden, A. M., Webster, T., & Stewart, H. (2013). Use of GIS and high resolution LiDAR in salt marsh restoration site suitability assessments in the upper Bay of Fundy, Canada. *Wetlands ecology and management*, 21(4), 243-262.
- Nash, J. E., & Sutcliffe, J. V. (1970). River flow forecasting through conceptual models part I—A discussion of principles. *Journal of hydrology*, 10(3), 282-290.
- NLHO. (2013). *Representatief Bathymetrisch Bestand* [Bathymetry data].
- Oost, A. P. (1995). *Dynamics and sedimentary developments of the Dutch Wadden Sea with a special emphasis on the Frisian Inlet: a study of the barrier islands, ebb-tidal deltas, inlets and drainage basins*: Faculteit Aardwetenschappen.
- Pope, S. B. (2001). *Turbulent Flows*, Cambridge University Press, Cambridge, UK. 125, 1361-1362.
- Poppema, D. W., Willemsen, P. W., de Vries, M. B., Zhu, Z., Borsje, B. W., & Hulscher, S. J. (2019). Experiment-supported modelling of salt marsh establishment. *Ocean & coastal management*, 168, 238-250.
- RWS. (2019). *water-info*. Retrieved from: waterinfo.rws.nl
- Schuerch, M., Spencer, T., & Evans, B. (2019). Coupling between tidal mudflats and salt marshes affects marsh morphology. *Marine Geology*, 412, 95-106.
- Silinski, A., Fransen, E., Bouma, T. J., Meire, P., & Temmerman, S. (2016). Unravelling the controls of lateral expansion and elevation change of pioneer tidal marshes. *Geomorphology*, 274, 106-115. doi:10.1016/j.geomorph.2016.09.006
- van Kessel, T., Spruyt-de Boer, A., van der Werf, J., Sittoni, L., van Prooijen, B., & Winterwerp, H. (2012). Bed module for sand-mud mixtures
- Van Ledden, M., Van Kesteren, W., & Winterwerp, J. (2004). A conceptual framework for the erosion behaviour of sand–mud mixtures. *Continental Shelf Research*, 24(1), 1-11.
- Van Loon-Steensma, J. M., & Slim, P. A. (2012). The impact of erosion protection by stone dams on salt-marsh vegetation on two Wadden Sea barrier islands. *Journal of Coastal Research*, 29(4), 783-796.
- Van Rijn, L. C. (1993). Principles of sediment transport in rivers, estuaries and coastal seas. 1006.
- Van Rijn, L. C. (2000). General view on sand transport by currents and waves: data analysis and engineering modelling for uniform and graded sand (TRANSPOR 2000 and CROSMOR 2000 models). Z2899.
- Vuik, V., Borsje, B. W., Willemsen, P. W., & Jonkman, S. N. (2019). Salt marshes for flood risk reduction: Quantifying long-term effectiveness and life-cycle costs. *Ocean & coastal management*, 171, 96-110.
- Vuik, V., Jonkman, S. N., Borsje, B. W., & Suzuki, T. (2016). Nature-based flood protection: The efficiency of vegetated foreshores for reducing wave loads on coastal dikes. *Coastal engineering*, 116, 42-56.
- Wamsley, T. V., Cialone, M. A., Smith, J. M., Atkinson, J. H., & Rosati, J. D. (2010). The potential of wetlands in reducing storm surge. 37(1), 59-68.
- Willemsen, P. W. J. M., Borsje, B. W., Hulscher, S. J. M. H., Van der Wal, D., Zhu, Z., Oteman, B., . . . Bouma, T. J. (2018). Quantifying Bed Level Change at the Transition of Tidal Flat and Salt Marsh: Can We Understand the Lateral Location of the Marsh Edge? *Journal of Geophysical Research-Earth Surface*, 123(10), 2509-2524. doi:10.1029/2018jf004742

- Willemsen, P. W. J. M., Horstman, E., Borsje, B. W., Friess, D., & Dohmen-Janssen, C. M. (2016). Sensitivity of the sediment trapping capacity of an estuarine mangrove forest. *Geomorphology*, *273*, 189-201.
- Willmott, C. J. J. P. g. (1981). On the validation of models. *2*(2), 184-194.
- Woth, K., Weisse, R., & Von Storch, H. (2006). Climate change and North Sea storm surge extremes: an ensemble study of storm surge extremes expected in a changed climate projected by four different regional climate models. *Ocean Dynamics*, *56*(1), 3-15.
- Wright, J., Colling, A., & Park, D. (1999). *Waves, tides and shallow-water processes* (Vol. 4): Gulf Professional Publishing.
- Zijl, F., & Groenenboom, J. (2019). DCSM-FM; Concise model description.
- Zijl, F., Verlaan, M., & Gerritsen, H. (2013). Improved water-level forecasting for the Northwest European Shelf and North Sea through direct modelling of tide, surge and non-linear interaction. *Ocean Dynamics*, *63*(7), 823-847.
- Zijlema, M., Van Vledder, G. P., & Holthuijsen, L. (2012). Bottom friction and wind drag for wave models. *Coastal engineering*, *65*, 19-26.
- Zwarts, L., Dubbeldam, W., van den Heuvel, H., van de Laar, E., Menke, U., Hazelhoff, L., & Smit, C. (2004). *Bodemgesteldheid en mechanische kokkelvisserij in de Waddenzee*: Rijkswaterstaat Rijksinstituut voor Kust en Zee/RIKZ.